International Journal of Naval Architecture and Ocean Engineering 11 (2019) 380–395

Contents lists available at ScienceDirect

International Journal of Naval Architecture and Ocean Engineering

journal homepage: http://www.journals.elsevier.com/international-journal-of-naval-architecture-and-ocean-engineering/

Bilge keel design for the traditional fishing boats of Indonesia's East Java

Wendi Liu [a, *], Yigit Kemal Demirel [a], Eko Budi Djatmiko [b], Setyo Nugroho [b], Tahsin Tezdogan [a], Rafet Emek Kurt [a], Heri Supomo [b], Imam Baihaqi [b], Zhiming Yuan [a], Atilla Incecik [a]

[a] Department of Naval Architecture, Ocean and Marine Engineering University of Strathclyde, Glasgow, UK
[b] Department of Naval Architecture and Shipbuilding, Marine Technology Faculty, Sepuluh Nopember Institute of Technology, Surabaya, Indonesia

ARTICLE INFO

Article history:
Received 23 February 2018
Received in revised form
17 July 2018
Accepted 17 July 2018
Available online 9 August 2018

Keywords:
East Java Fishing Boat
Bilge keel
Roll motion

ABSTRACT

Seakeeping, especially for the roll motions, is of critical importance to the safe operation of fishing boats in Indonesia. In this study, a traditional East Java Fishing Boat (EJFB) has been analysed in terms of its seakeeping performance. Furthermore, a bilge keel was designed to reduce the roll motions of the EJFB using multiple stages approach. After installing the designed bilge keels, it was shown that up to 11.78% and 4.87% reduction in the roll response of irregular seaways and the total resistance under the design speed, respectively. It was concluded that the roll-stabilized-EJFB will enhance the well-being of the fisherman and contribute to the boats' safe operation, especially in extreme weather conditions. Moreover, the total resistance reduction of the EJFB due to the installation of the designed bilge keels also resulted in increased operational efficiency and reduced fuel costs and fuel emissions for local stakeholders.

1. Introduction

Fishing is extremely important for Indonesia, with around 6.4 million people participating in fishing activities. Indonesia is reported to have approximately 700,000 fishing boats, of which 25% are dugout canoes and 50% are without motors (Liu et al., 2016). Currently, a fleet of traditional fishing boats made from solid woods has been in service for a long time. As an evidence, Fig. 1 shows an illustration of fishing boats at the fishing port of Panceng in Gresik, which is a centre fishing port in East Java, Indonesia. Various types of traditional boats operate in the different regions of Indonesia, such as *Begog* boats in Madura, *Lambo* boats in South Sulawesi and *Phinisi* boats in some tourist attraction. East Java Fishing Boat (EJFB) is one of the most common types of fishing boats that services in the East Java. EJFB is widely used in East Java as a means of catching fish in the sea. EJFBs are still widely used by Indonesian fishermen, making up the majority of the fishing boat population in various Fish Landing Sites (FLS) in East Java.

The literature shows that the hydrodynamic performance of the traditional EJFBs has not been tested to date. There are many traditional boatbuilding companies in Indonesia, and most of them are still using outdated methods to design these traditional EJFBs, which are based on traditional practices and experiences. It is, therefore, necessary to perform hydrodynamic and seakeeping analyses for such local boats so that their safety, efficiency and performance can be enhanced and optimized.

Fishing is a labour intensive and difficult job, which generally attracts workers from the less privileged parts of society. Most fishermen work under harsh conditions with boats not completely fit for purpose (Arslan et al., 2016; OGP, 2010). This has a drastic negative impact on safety, and, as a result, most global maritime accidents occur in fishing boats, with many lives lost every year (Turan et al., 2016). In order to maximize the safety and efficiency of EJFBs, a major optimization and safety/performance enhancement of these boats is required. Such a large-scale optimization and safety/performance enhancement requires an extensive study encompassing all aspects of boat design, such as hydrodynamics, structure, manufacturing and construction.

Roll motion has a significant impact on the safety and performance of operating boats by reducing the effectiveness of the fishermen as well as the onboard equipment (Perez and Blanke,

* Corresponding author.
E-mail address: wendi.liu@strath.ac.uk (W. Liu).
Peer review under responsibility of Society of Naval Architects of Korea.

https://doi.org/10.1016/j.ijnaoe.2018.07.004

Fig. 1. Fishing boat at fishing port of Panceng, Gresik, Indonesia.

2010). Furthermore, the boat has the risk of capsizing due to the large roll motion under extreme sea and weather conditions. Thus, there is a need to analyse the roll responses of EJFB and use roll stabilization techniques to reduce the roll amplitude if necessary. Roll damping is a key parameter when calculation roll displacements, especially if the boat operates in the moderate to extreme sea conditions (Bassler and Reed, 2009). Roll damping is highly non-linear and is affected by several complex phenomena such as the interactions between boat hull and fluid flows, which are hard to predict (Chakrabarti, 2001).

There are several devices designed to reduce roll motion including bilge keels, antiroll fins and antiroll tanks (Cox and Lloyd, 1977). Among all roll stabilizers, bilge keels are the most suitable type for the EJFB since they are much simpler to design and install. Unlike the antiroll fin and the antiroll tank, bilge keels do not take up any cabin space and do not need to be actively operated during a boat's operation. These features make bilge keels very suitable for the EJFB. Bilge keels are widely used for modern large ships, such as large cargo vessels. However, it is not a common practice to use bilge keels for a traditional small wooden boat. Therefore, a thorough design optimization study is necessary to obtain maximum benefit from a bilge keel to be installed to a traditional fishing boat such as EJFB in this study.

As reported by Cox and Lloyd (1977), a traditional bilge keel design method contains various steps. The first step is to determine the roll characteristics of the selected boat in a wide range of decay coefficient values. The second step is to determine the roll decay coefficient of the bilge keel for different combinations of the bilge keel length and span. Lastly, the parameter of fitted bilge keels for the boat could be obtained through the objective decay coefficient. This traditional bilge keel design method is based on empirical formulae. It is a fast and efficient way a bilge keel design but it contains large uncertainties for the performance of the bilge keel to be used. Our literature survey revealed that a modern design method, which employs high fidelity techniques, is required for bespoke bilge keels for any kind of ships.

In this study, a bilge keel was designed for a conventional fishing boat operating in Indonesia (EJFB). This can be seen as the first practice of using bilge keels for traditional small bamboo/wooden boats. In this study, an optimization of a modern bilge keel design method that employs high fidelity techniques based on the total resistance and roll motions was presented and applied to the design of the roll-stabilized-EJFB. The present study also filled the gap of the lack of hydrodynamic and seakeeping analyses of the widely used traditional fishing boat, EJFB in Indonesia. The calm water total resistance of the EJFB was obtained using a state-of-the-art Computational Fluid Dynamics (CFD) technique. STAR-CCM+, which is a commercial CFD software package, was used as a RANS solver. In the interest of time, the seakeeping analysis (in regular and irregular waves) was performed using a potential flow-based software package (ShipX). The resistance of the roll-stabilized-EJFB and the bilge keel geometry were also modelled in STAR-CCM+ and ShipX as parts of the bilge keel design, respectively.

This paper is organized as follows. The methods, formulae, validation and verification used in the present study are presented in Section 2. The main characteristics of the EJFB and its seakeeping ability are given in Section 3. The procedure of bilge keel design is explained in every detail in Section 4. Section 5 presents the performance of the designed bilge keel in terms of the roll stabilization ability in irregular waves and the resistance difference. Finally, concluding remarks are summarised in Section 6.

2. Methodology

The present study employs multiple stages for the bilge keel design. A flowchart on the procedure of the roll-stabilized EJFB (bilge keel) design is shown in Fig. 2. The design methodology starts with the parameter determination to generate design cases through predetermined ranges for each parameter. The second step is to set several design criteria, based on published references, to screen out unsuitable design cases. The third step employs the conventional strip theory formulations to analyse the roll stabilization performance of every bilge keel design case in regular waves. The best-performed design case will be selected as the final bilge keel design. The seakeeping performance of the roll-stabilized-EJFB with the final bilge keel geometry in irregular waves will be analysed anew using the conventional strip theory formulations in step 4. In step 5, the calm water resistance of the roll-stabilized-EJFB will be calculated and compared with that of the EJFB bare hull by using CFD method.

ShipX software is used to implement the conventional strip theory formulations in step 3 and 4 for the seakeeping analysis of the EJFB in both regular and irregular wave conditions in the frequency domain. The detail formulations of the conventional strip theory used in the present study are presented in Section 2.1 and 2.2 for the regular and irregular wave conditions, respectively. In step 5, an Unsteady Reynolds-Averaged Navier-Stokes (URANS) method was used to solve the governing equations in this study. These mass and momentum conservation equations were solved by the commercial CFD software STAR-CCM+ (CD-Adapco, 2014) and the details are presented in Section 2.3.

2.1. Boat response in regular waves

The seakeeping analysis in the present study assumes that the wave-amplitude is relatively small compared with the dimensions of the boat and the wave steepness is small enough to avoid wave breaking. As mentioned earlier, the seakeeping calculation was performed using ShipX, which is based on linear strip theory. It assumes a linear relationship between the wave loads/motions and the wave amplitudes. Steady-state conditions are also used so as to assume a harmonic oscillation of the boat's linear dynamic loads that have the same frequency as the wave excited loads (Fathi and Hoff, 2004). The linear coupled differential equations of boat motion are written as

$$\sum_{k=1}^{6}\left[\left(M_{jk}+A_{jk}\right)\ddot{\eta}_k+B_{jk}\dot{\eta}_k+C_{jk}\eta_k\right]=F_j e^{i\omega t},\ \ j=1,\ \cdots,6 \qquad (1)$$

where M_{jk} is the generalized mass matrix, A_{jk} is the added mass matrix, B_{jk} is the linear damping matrix, C_{jk} is the stiffness matrix and F_j is the complex amplitudes of the wave exciting forces and

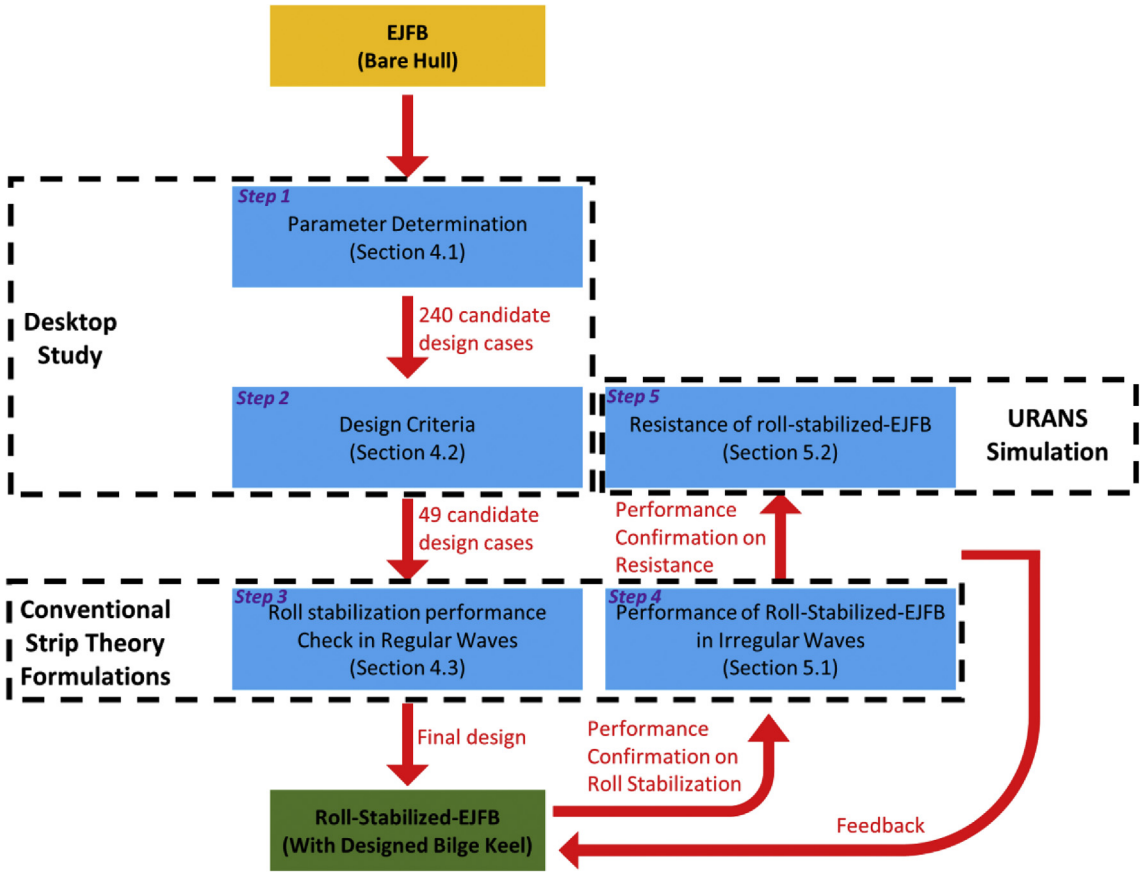

Fig. 2. Flowchart of the Bilge Keel design for the EJFB.

moments. F_1, F_2 and F_3 refer to the surge, sway and heave amplitude of exciting forces, while F_4, F_5 and F_6 refer to the roll, pitch and yaw amplitude of exciting moments, respectively. ω is the angular frequency of encounter, which is calculated as

$$\omega = \omega_0 + \frac{\omega_0^2 U}{g}\cos\beta \tag{2}$$

where ω_0 is the wave frequency, U is the speed of the boat and g is the gravitational acceleration. η_k is the motion responses. η_1, η_2, η_3, η_4, η_5 and η_6 refer to the surge, sway, heave, roll, pitch and yaw motions, respectively. β is the heading angle between the vessel and the wave propagation direction. Here $\beta = 0^\circ$ is head seas, $\beta = 90^\circ$is beam seas and $\beta = 180^\circ$is following sea.

The linear coupled differential motion equation could be solved by substitutions of

$$\eta_k = \tilde{\eta}_k e^{i\omega t}, \quad k = 1, \cdots, 6 \tag{3}$$

where $\tilde{\eta}_k$ is the complex motion amplitude.

The roll motion calculation is an important part of this study. The roll motion is calculated as

$$\begin{aligned}&(M_{42} + A_{42})\ddot{\eta}_2 + B_{42}\dot{\eta}_2 + (M_{44} + A_{44})\ddot{\eta}_4 + \left(B_{44}^{P} + B_{44}^{V1}\right)\dot{\eta}_4 \\ &+ B_{44}^{V2}|\dot{\eta}_4|\dot{\eta}_4 + C_{44}\eta_4 + (M_{46} + A_{46})\ddot{\eta}_6 + B_{46}\dot{\eta}_6 \\ &= F_4\end{aligned} \tag{4}$$

where the superscripts P, $V1$ and $V2$ refer to the potential linear and quadratic viscous damping terms, respectively. Due to these terms, the roll equation is non-linear and an iteration method must be used to solve it. Generally, the roll damping includes three components: frictional damping, eddy damping and stabilizer (i.e. bilge keel) damping (Fathi and Hoff, 2004; Himeno, 1981).

The calculation of the bilge keel damping includes two components: damping generated by the normal forces of the bilge keel and the damping generated by the bilge keel induced hull pressure. The damping generated by the normal forces of the bilge keel is calculated based on Ikeda et al. (1977) as follows:

$$B_{44}^{V1} = \frac{8}{3\pi^2}\cdot 22.5 \cdot b_{bk}^2 \cdot r_{bk}^2 \cdot f \cdot \omega \tag{5}$$

and

$$B_{44}^{V2} = 2.4 \cdot b_{bk} \cdot f^2 \cdot r_{bk}^3 \tag{6}$$

where b_{bk} is the width of the bilge keel, r_{bk} is the length between the roll axis, the bilge keel and f is the correction factor for the velocity increment at the bilge keel.

2.2. Boat response in irregular waves

The ship responses to an irregular seaway were calculated using the spectral technique of St Denis and Pierson (1953). The motion responses of the boat to the natural irregular seas (S_Z) are calculated by using the seaway spectrum (S_ζ) and the transfer functions in the frequency domain with the linear superposition principle.

Based on the field study and literature review, the sea state in East Java follows the JONSWAP spectrum, with the wave height

varying from 0.3 m to 1.88 m and the corresponding wave period varying from 7 s to 9 s (Djatmiko, 2015; Tezdogan et al., 2014). The peak-enhancement factor is taken to be 2 which reflects the real sea conditions in the East Java in Indonesia.

2.3. CFD calculations

CFD calculations were performed in the present study to calculate the resistance of the EJFB in calm water at its service speed. The averaged continuity and momentum equations for incompressible flows without body forces are shown in tensor form and Cartesian coordinates as follows (Ferziger and Peric, 2002):

$$\frac{\partial(\rho\overline{u}_i)}{\partial x_i} = 0 \tag{7}$$

$$\frac{\partial(\rho\overline{u}_i)}{\partial t} + \frac{\partial\left(\rho\overline{u}_i\overline{u}_j + \rho\overline{u_i^{'}u_j^{'}}\right)}{\partial x_j} = -\frac{\partial\overline{p}}{\partial x_i} + \frac{\partial\overline{\tau_{ij}}}{\partial x_j} \tag{8}$$

where τ_{ij} is the mean viscous stress tensor components as

$$\overline{\tau}_{ij} = \mu\left(\frac{\partial\overline{u}_i}{\partial x_j} + \frac{\partial\overline{u}_j}{\partial x_i}\right) \tag{9}$$

p is the mean pressure, $\overline{u}_i$ is the averaged Cartesian components of the velocity vector, $\rho\overline{u_i^{'}u_j^{'}}$ is the Reynolds stresses, ρ is the fluid density and μ is the dynamic viscosity.

The finite volume method was employed to solve the Navier-Stokes equations. The continuity and momentum equations of the Navier-Stokes equations were linked by the predictor-corrector approach of the RANS solver.

The standard k-ε turbulence model is relatively economical in terms of CPU time compared with other two-equation turbulence models and has been used extensively for industrial applications (CD-Adapco, 2014) and many other studies in the same area (Kim and Lee, 2011; Enger et al., 2010). Thus, the standard k-ε model was selected for the present study. The VOF method was used to accurately capture the free surface with a second-order convection scheme. The segregated flow model was applied to the simulations. The unsteady term of the RANS formula was discretized by the first-order temporal scheme. Convection terms in the RANS formula were discretized by applying a second-order upwind scheme. The overall solution procedure was obtained according to a SIMPLE-type algorithm. A Dynamic Fluid Body Interaction (DFBI) model was used to simulate realistic boat behaviour, which allowed the boat to be free to move in the pitch and heave directions due to the exciting force and moments acting on the boat hull (CD-Adapco, 2014).

In each cell of the present simulations, the Courant number (CFL), which is defined as below, was kept as less than or equal to one for numerical stability.

$$CFL = \frac{U\Delta t}{\Delta x} \tag{10}$$

where Δt is the physical time step, Δx is the mesh cell dimension and U is the mesh flow speed.

A general view of the computational domain with the EJFB model and the notations of selected boundary conditions are depicted in Fig. 3. Only half of the hull (the port side) is represented to reduce the computational complexity and demand. The symmetry plane forms the centreline domain face in order to accurately simulate the other half of the model. The mirror image of the boat and domain in some figures given hereafter is reflected on the starboard side for plotting purposes.

As illustrated in Fig. 3, the positive x-direction was set in the velocity inlet boundary condition. The pressure outlet was modelled in the negative x-direction. Velocity inlets were applied to the top and bottom boundaries. The symmetry condition was applied in the symmetry plane, and the side of the domain (the negative y-direction) has a velocity inlet boundary condition. These boundary conditions were used as they gave the quickest flow solutions for similar simulations carried out utilising Star-CCM+ (CD-Adapco, 2014). The velocity inlet boundary condition was selected for the top and bottom boundaries so as to reflect the deep water and open sea conditions. Since the pressure outlet boundary condition prevents backflow from occurring and fixes static pressure at the outlet, it was applied to the boundary behind the boat. The

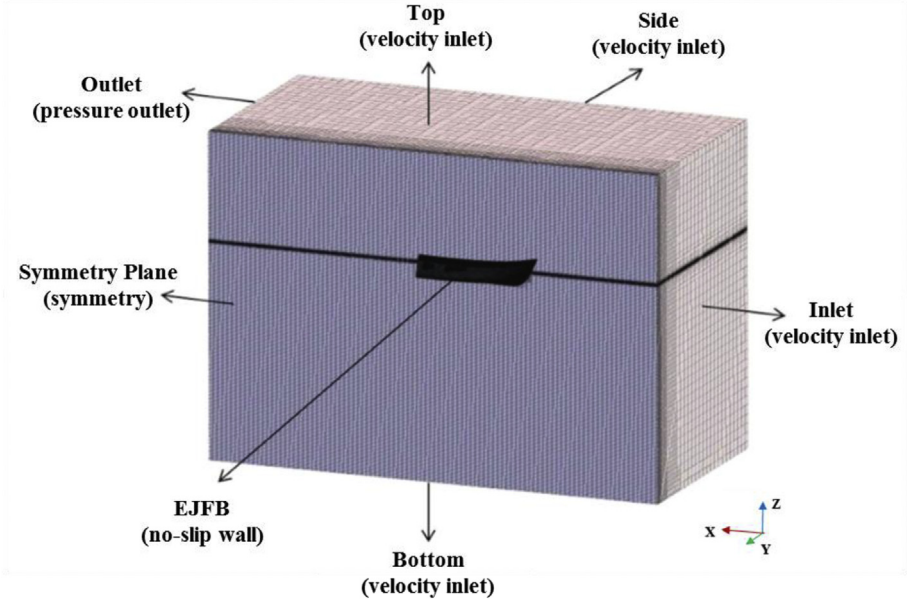

Fig. 3. A general view of the domain and the applied boundary conditions of CFD simulations.

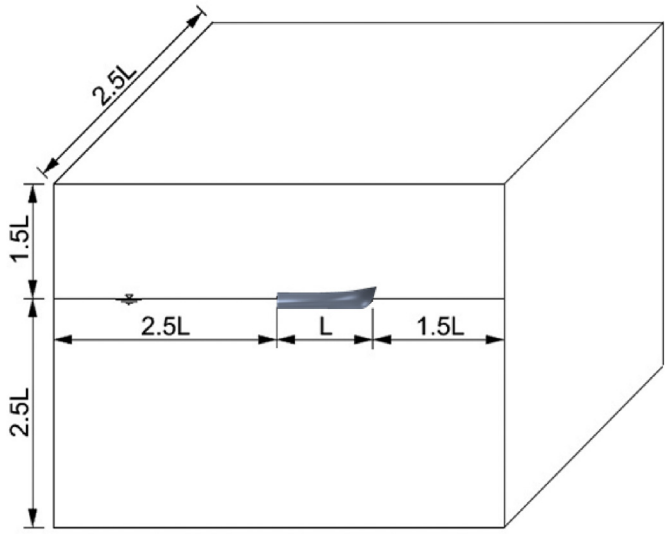

Fig. 4. The dimensions of the computational domain for the CFD simulations.

locations of the boundaries are illustrated in Fig. 4. The outlet boundary was located 2.5L (L represents the length between perpendiculars of the EJFB) away from the boat hull to prevent any reflective waves by the boat, based on the recommendations in CD-ADAPCO (CD-Adapco, 2014).

The calculation mesh was generated using the automatic meshing facility in STAR-CCM+, which uses the Cartesian cut-cell method, resulting in a computational mesh of circa 2.2 million cells in total. A high-quality mesh formed primarily of unstructured hexahedral cells was obtained with the trimmed cell mesher. The area around the EJFB hull, the expected free surface and the wake of the EJFB were progressively refined in the mesh size so as to ensure the complex flow features could be appropriately captured. The cross-section of the computational mesh in both the x-y plane and the x-z plane is shown in Fig. 5. The surface mesh on the EJFB hull is shown in Fig. 6.

2.4. Validation and verification

For the validation and verification of the methodology employed in this study, two approaches were utilised. The validation of ShipX (for seakeeping calculations) was carried out with a Wigley III hull against experimental data, which are freely available in the literature. The verification of this study's CFD work was performed with the actual EJFB. As no experimental data are available for this boat, comparison of the simulated results with experiments was not possible. However, it should be noted that the CFD technique utilised in this study was validated earlier by the same authors with different ship geometries and under different conditions (Tezdogan et al., 2015).

Seakeeping calculations were performed for the case of Wigley III hull advancing in a head sea condition. The obtained numerical results were compared with published experimental (Journée,

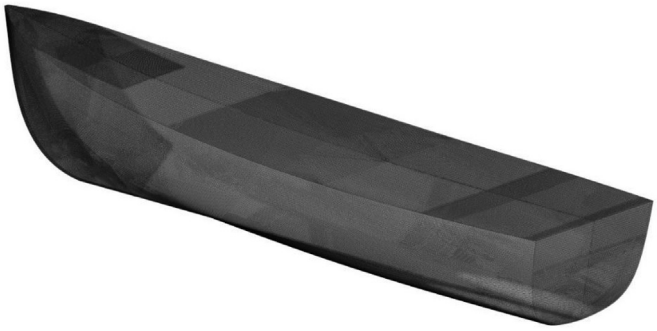

Fig. 6. Surface mesh on the EJFB hull for CFD simulation.

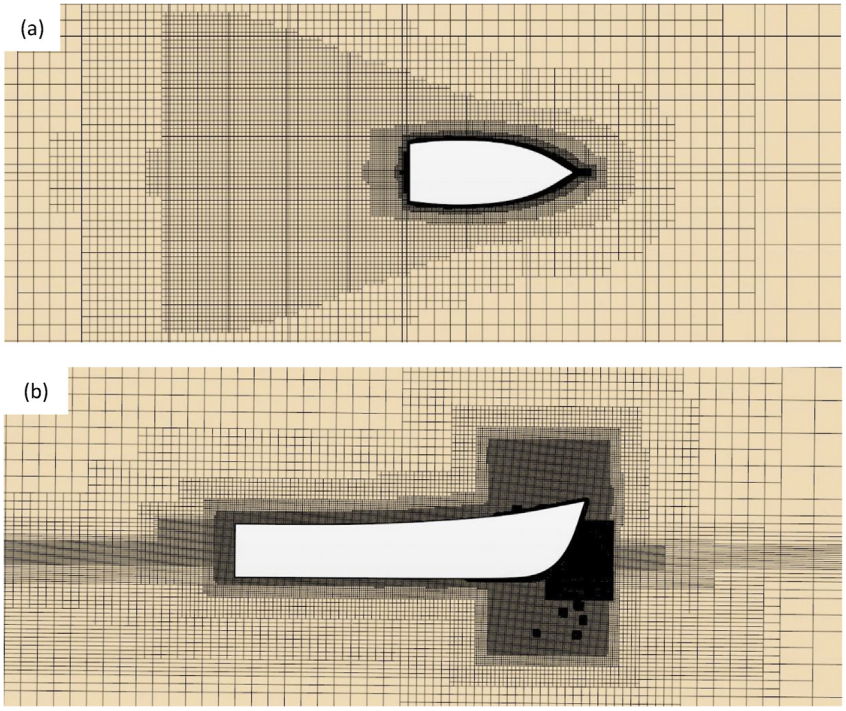

Fig. 5. Cross-section of the computational mesh for the CFD calculation (a) in X-Y plane and (b) in X-Z plane.

Table 1
General properties of Wigley III hull for validation purposes.

Main dimensions of Wigley III hull	
Length, *Lt* (m)	3
Breadth, *B* (m)	0.3
Draught, *D* (m)	0.1875
Displacement, *V* (m^3)	0.078
Centre of rotation above base, *KR* (m)	0.1875
Centre of gravity above base, *KG* (m)	0.17
Radius of inertia for pitch, *kyy* (m)	0.75

1992) and numerical results (Yuan et al., 2014) as a validation. The Wigley III hull is modelled based on the equation below and corresponding particulars of the Wigley III model are shown in Table 1.

$$y = \frac{B}{2}\left[1-\left(\frac{z}{D}\right)^{s}\right]\left[1-\left(\frac{2x}{L}\right)^{2}\right]\left[1+0.2\left(\frac{2x}{L}\right)^{2}\right] \tag{11}$$

As can be seen from Fig. 7 that the heave and pitch RAOs calculated by ShipX agree well with the model test results of Journée (1992) and the numerical calculations of Yuan et al. (2014), which proves the accuracy of the present seakeeping calculation method.

In this study, a proper verification study was undertaken to show the capability of the proposed CFD model and the software for particular calculations. As indicated in the literature (Richardson, 1911; Richardson and Gaunt, 1927; Celik et al., 2008; Demirel et al., 2017), the Grid Convergence Index (GCI) Method was used to estimate the discretisation error. The Grid Convergence Index for a fine-grid is calculated as:

$$GCI_{fine}^{21} = \frac{1.25e_a^{21}}{r_{21}^{p_a}-1} \tag{12}$$

where e_a^{21} is the approximate relative errors. It is calculated by using the following equation

$$e_a^{21} = \left|\frac{\varphi_1-\varphi_2}{\varphi_1}\right| \tag{13}$$

and corresponding extrapolated relative error is calculated as

$$e_{ext}^{21} = \left|\frac{\varphi_{ext}^{12}-\varphi_1}{\varphi_{ext}^{12}}\right| \tag{14}$$

φ_k is the key variable in the k^{th} grid. The φ_k represents C_T in the present study. The extrapolated value, φ_{ext}, is obtained by

$$\varphi_{ext}^{21} = \frac{r_{21}^{p_a}\varphi_1-\varphi_2}{r_{21}^{p_a}-1} \tag{15}$$

The apparent order of the method, denoted as p_a, is obtained by

$$p_a = \frac{1}{\ln(r_{21})}\left|\ln\left|\frac{\varepsilon_{32}}{\varepsilon_{21}}\right| + q(p_a)\right| \tag{16}$$

where q is calculated as

$$q(p_a) = \ln\left(\frac{r_{21}^{p_a}-s}{r_{32}^{p_a}-s}\right) \tag{17}$$

and s is calculated as

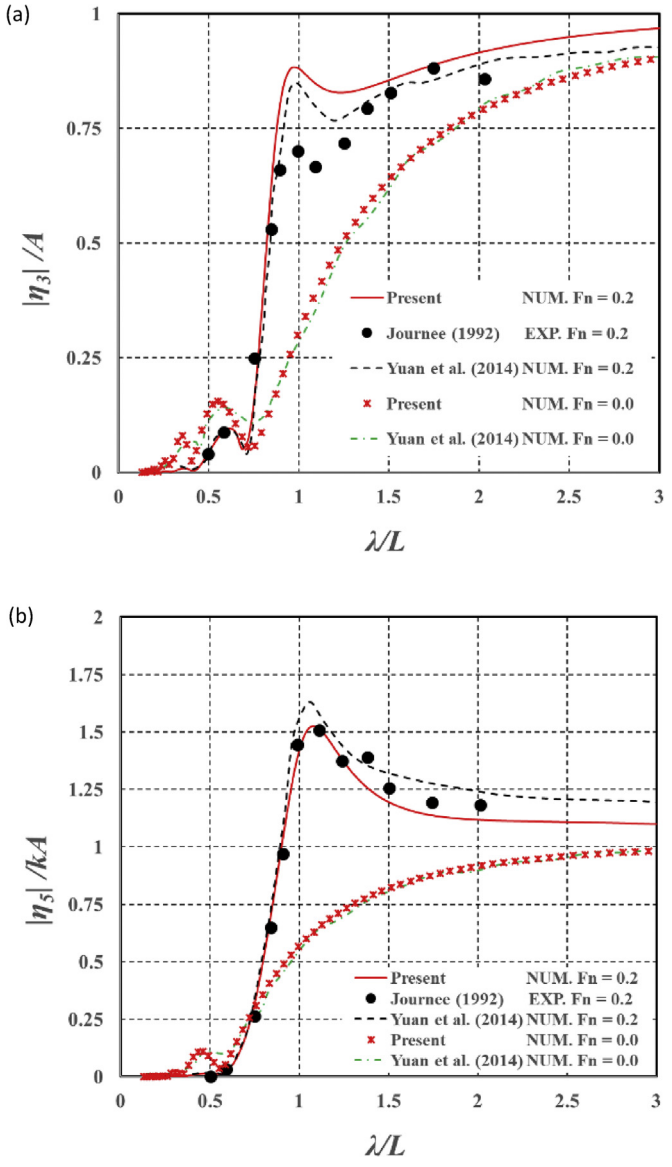

Fig. 7. Validation results on non-dimensional (a) heave and (b) pitch response amplitude at both $Fn = 0.2$ and $Fn = 0$.

$$s = 1 \cdot \sin\left(\frac{\varepsilon_{32}}{\varepsilon_{21}}\right) \tag{18}$$

with ε_{32} and ε_{21} obtained as

$$\varepsilon_{32} = \varphi_3 - \varphi_2 \tag{19}$$

and

$$\varepsilon_{21} = \varphi_2 - \varphi_1 \tag{20}$$

The refinement factors r_{21} and r_{32} take the value of $\sqrt{2}$ in the present study.

The values of parameters in the GCI calculation were obtained for the C_T of the EJFB and are presented in Table 2.

It is clear from Table 2 that numerical uncertainties for the C_T of the EJFB are 0.56521%, which is acceptable for further EJFB simulations using the present CFD model.

Table 2
Calculation of the discretisation error for C_T values of the EJFB.

Parameters	C_T
r_{21}, r_{32}	$\sqrt{2}$
φ_1	0.028171
φ_2	0.028379
φ_3	0.028458
p_a	2.7933
φ_{ext}^{21}	0.028044
e_a^{21}	0.73835%
e_{ext}^{21}	0.45422%
GCI_{fine}^{21}	0.56521%

3. Characteristics of the traditional EJFB

As mentioned in Section 1, the present study focuses on the roll amplitude reduction of EJFB, a traditional fishing boat in Indonesia. The body plan of the full-scale EJFB model is presented in Fig. 8. Corresponding main properties of the boat are listed in Table 3.

The service speed of the EJFB is 8 knots (4.11 m/s), which corresponding Froude number (Fn) is 0.57. After discussions with local fishermen and fishing-boat yard owners during a field study in Indonesia, the operational profile of the EJFB was obtained as follows: A typical sailing for the EJFB lasts about 12 h in total, including sailing at the service speed for 9–10 h and standby (at zero speed) for 2–3 h. Since the duration of the accelerating, decelerating and standby stages of the EJFB are much smaller than the duration of the EJFB at its service speed, the safety of the EJFB during the cruising stage at its service speed is much more important. Thus, the present study focuses on the seakeeping analysis and bilge keel design under service speed (8 knots) condition.

The ship responses to regular waves were calculated in the frequency domain at the service speed. The Response Amplitude Operators (RAOs) were predicted for five different wave headings, varying from a head sea condition to a following sea condition. The results of six RAOs are shown in Fig. 9. The linear responses, which are surge (η_1), sway (η_2) and heave (η_3), all with units of metres, are rendered dimensionless by the wave amplitude (A). The angular responses, which are roll (η_4), pitch (η_5) and yaw (η_6), all with units of radians, are rendered dimensionless by the wave slope (kA), where k is the wave number. All responses in Fig. 9 are plotted against the dimensionless wavelength (λ/L), where λ is the wavelength in metres and L is the length between perpendiculars of the EJFB.

It can be seen from Fig. 9 that the maximum sway, heave and yaw amplitudes are reached with a wave heading of 135° and dimensionless wavelength around 1.1. The maximum surge and pitch amplitudes are excited by following sea conditions, but with dimensionless wavelengths of 1.75 and 2.35, respectively. It should be noted that in this study a wave heading of 0° corresponds to a head sea condition.

From the roll response results at $Fn = 0.57$, both head sea and following sea conditions are not excited by any roll motions, which is in line with common sense. The peak value of the roll response under the beam sea condition and wave heading of 135° condition is around $\lambda/L = 1.0$. The maximum roll response is achieved under wave heading of 45° condition at $\lambda/L = 2.35$, which is 1.5 and 2.4 times larger than that with the beam sea condition and wave heading of 135° condition, respectively. Thus, there is a need to reduce such large roll amplitude of the EJFB, especially for the wave heading of 45° condition, so as to enhance the safety of the EJFB during operation. In the following sections, a roll stabilizer, more specifically a bilge keel, will be designed with an aim to reduce the roll response.

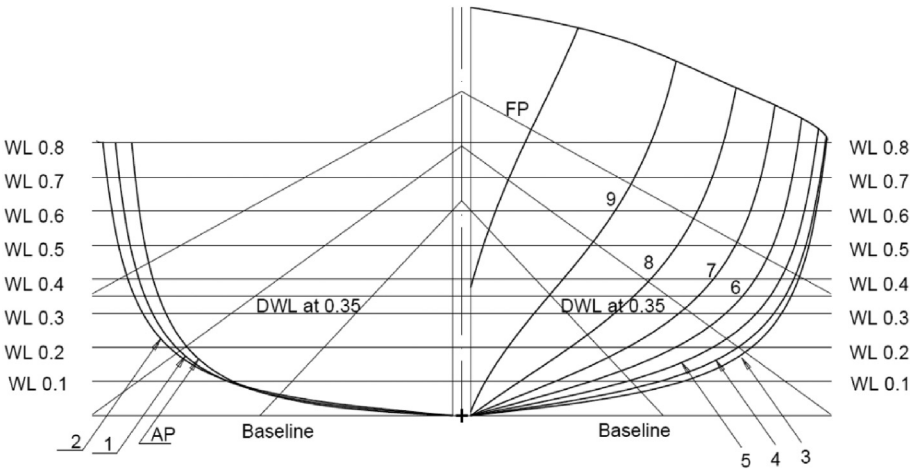

Fig. 8. Body plan of the EJFB.

Table 3
EJFB general properties.

Main properties of the EJFB			
Length betw. perp.	L	[m]	5
Breadth	B	[m]	1.934
Loaded draft	T	[m]	0.35
Displacement	Δ	[t]	1.9
Block coefficient	C_B	[−]	0.5367
Mid-boat section coefficient	C_M	[−]	0.764
Prismatic coefficient	C_P	[−]	0.7025

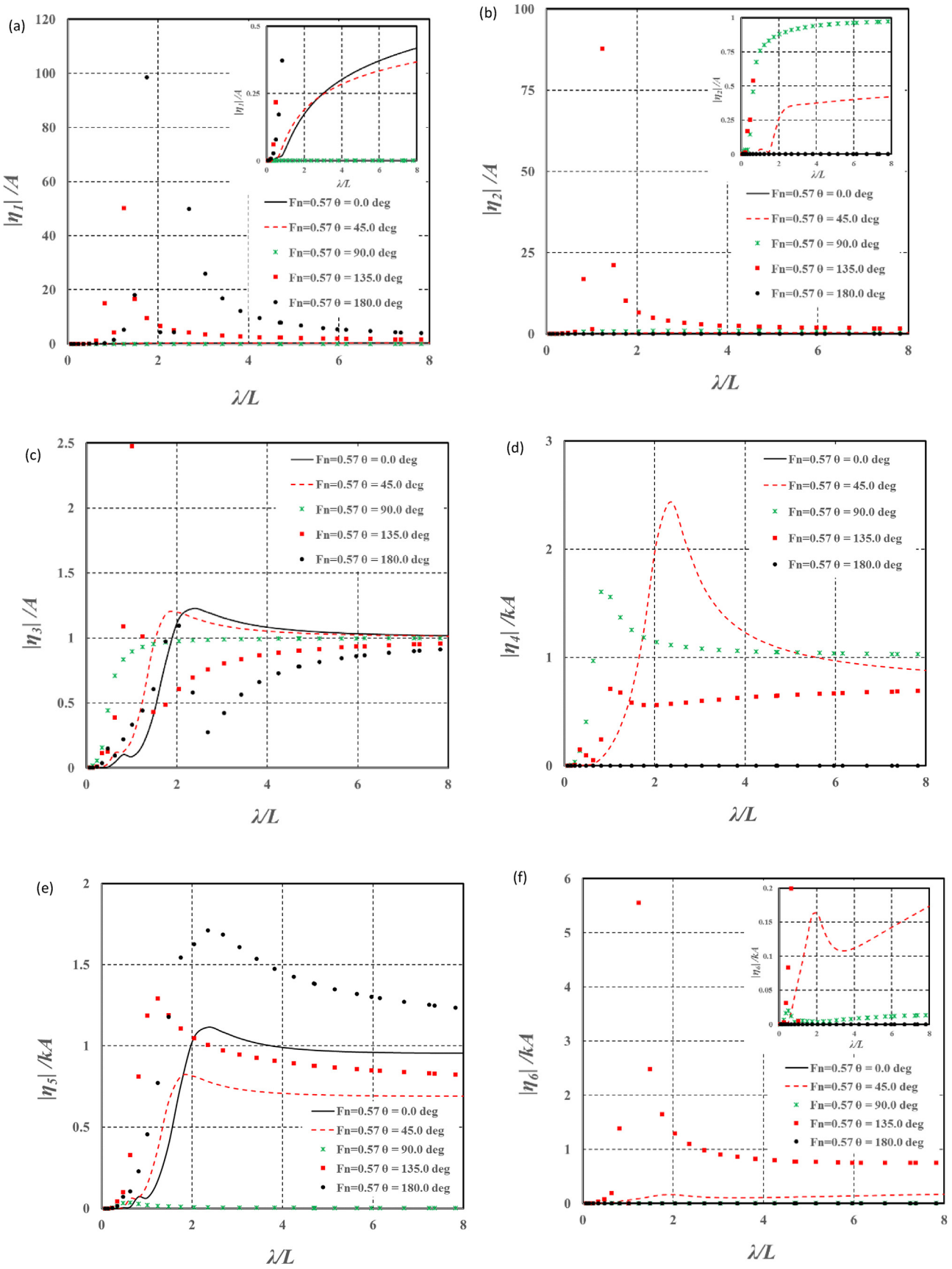

Fig. 9. Six RAOs of the EJFB at $Fn = 0.57$ for different wave headings.

A CFD simulation was run for the EJFB under calm water at service speed (8 knots). The free surface of the water (demonstrated as purple iso-surface) and flow streamlines (coloured by velocity magnitude of fluid particles) from bow to stern around the boat hull are illustrated in Fig. 10. The flow run-up phenomenon can be seen from the boat bow. The streamlines around the boat hull should be carefully investigated for bilge keel design, which will be discussed in detail in the following sections.

4. Bilge keel design for the roll stability enhancement of the EJFB

As stated previously, this study focuses on the reduction of the roll motion of the EJFB by the instalment of a bilge keel. Compared with other active or passive roll stabilizers, such as anti-roll fins and anti-roll tanks, bilge keels are much easier in terms of construction, especially for EJFB builders, and they do not need any additional operations to be performed by fishermen during the sailing course. In this section, the design stages of a bilge keel for the EJFB operating in the Indonesian seas are explained with all necessary details.

4.1. Design parameters of the bilge keel

A complete methodology for the parameter determination of the designed bilge keel is described in this section.

4.1.1. Shape and transverse location of bilge keel

It is widely accepted that the shapes of bilge keels have to follow the flow streamlines around a boat's hull so as to achieve better performance and minimize the additional resistance of bilge keels caused by angle induced drag forces during its forward motion (Bhattacharyya, 1978). Thus, the shapes of the bilge keels that were designed for the EJFB in the present study follow the flow streamlines of the boat hull around the bilge position. As indicated by Lloyd (1989), flow visualization techniques are usually performed for the boat model during the design stage to obtain the flow streamlines around the boat hull. In the present study, CFD simulations were carried out in calm water to obtain the flow streamlines of the EJFB, as outlined in Section 3. As the flow streamlines vary with the forward speed, such alignment between bilge keel shapes and flow streamlines can only be achieved for one forward speed, which is usually the service speed. Since during EJFB sailing about 80% of the time is spent at service speed (8 knots), the resistance penalty during its accelerating and decelerating stages can be ignored. The bilge keel design for the EJFB is focused on the cruising stage at service speed in the present study.

It is necessary to identify a transverse location for the bilge keel so as to enlarge the moment arm and the roll damping of the bilge keel. It is also worth mentioning that the transverse location of the bilge keel has to be fully immersed into the water so as to avoid any wave making resistance generated by the interaction between the bilge keel and the free-surface. Dove (1958) carried out a series of roll decay experiments at zero forward speed for a fine-form frigate model, reporting a large difference in the roll damping that was provided by the bilge keel at different transverse locations. In Dove's study, it is stated that the maximum roll damping was achieved by the bilge keel when it was located one quarter along the girth from the free-surface to the baseline of the boat. Since the ideal transverse location of the bilge keel is highly related to the shape of the boat, Dove's results may not apply for EJFB. In order to identify the best transverse location of the bilge keels for the EJFB, 12 locations were selected, which are evenly distributed from the free-surface to the baseline, for further calculation. As shown in Fig. 11, twelve flow streamlines were selected as the candidate shape and potential transverse location of the bilge keels. A two-dimensional local coordinate system was established for these streamlines. The origin of this local system is located in the bottom of the stern. The x-axis follows the boat baseline and points to the boat bow and the z-axis direction is vertical up. The coordinates of the points that are located at each flow streamline were extracted within the aforementioned two-dimensional local coordinate system. With these extracted points/line data, 12 candidate combinations of bilge keel shape and transverse location were identified and are illustrated in Fig. 12.

In order to quantify these 12 transverse locations, Lc_{bk}/T was defined where Lc_{bk} is the averaged distance between the bilge keel and the baseline measured all along the bilge keel. Corresponding Lc_{bk}/T values for each transverse location are listed in Table 4.

4.1.2. Length and longitudinal location of bilge keel

The lengths of bilge keels are typically no less than 25% of the boat's length to secure a satisfactory performance with regards to the roll stabilizing (Bhattacharyya, 1978; Sabuncu, 1983). The maximum length of bilge keels varies from 50% of the boat's length (Bhattacharyya, 1978) to 75% of the boat's length (Sabuncu, 1983). In the present study, five bilge keel lengths (Lt_{bk}) were selected for further investigation: 25%L, 37.5%L, 50%L, 62.5%L and 75%L.

Following this, the longitudinal locations of each length option have to be defined. Generally, the bilge keel should be located within the middle one-third region of the boat length, when the length of the bilge keel is smaller than 33% of the boat's length (Cox and Lloyd, 1977). When the length of the bilge keel is larger than 33% of the boat's length, the middle one-third region should be covered primarily, and then the bilge keel extended to both the bow and stern sides. Lofft (1973) and Cox and Lloyd (1977) reported an

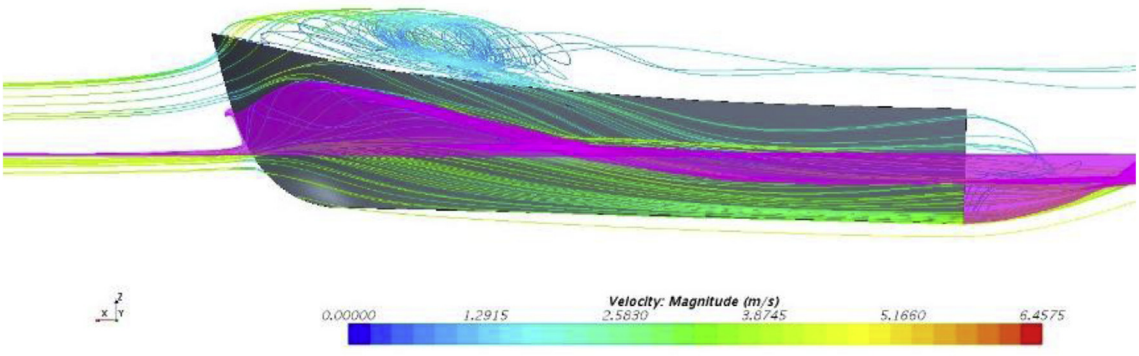

Fig. 10. Free-surface and flow streamlines around the EJFB at $Fn = 0.57$ in calm water.

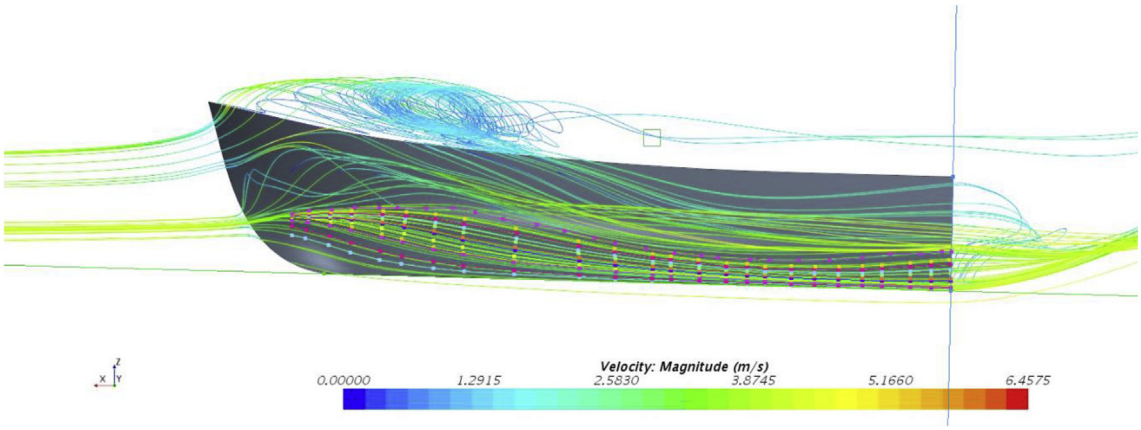

Fig. 11. Streamlines extraction for bilge keel design of EJFB based on the CFD calculation at $Fn = 0.57$ in calm water.

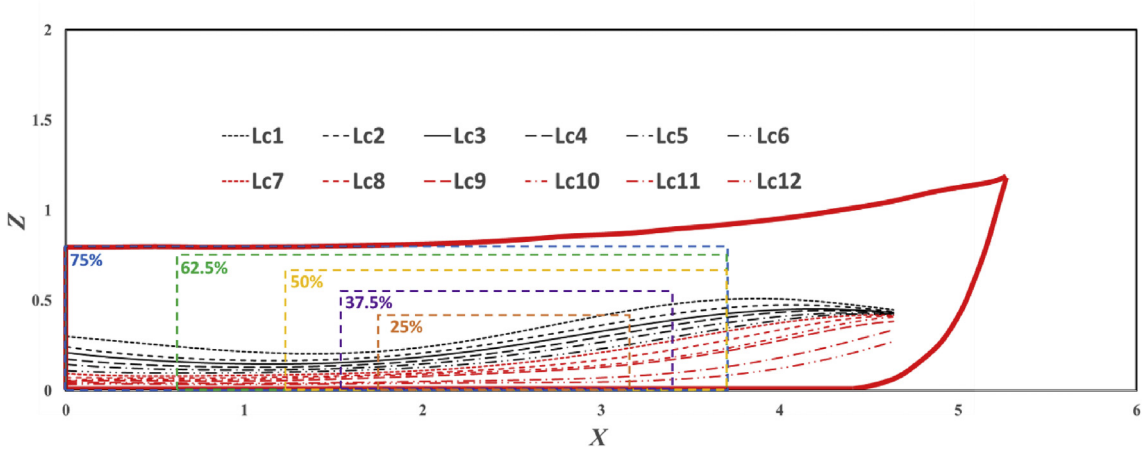

Fig. 12. Illustration of 12 bilge keel candidate locations and cut positions of 5 bilge keel candidate lengths.

Table 4
Average distance from baseline for 12 bilge keel candidate transverse locations and corresponding maximum width allowed within the boat envelope.

Location name	Average distance from baseline Lc_{bk}/T %	Maximum width allowed within the boat envelope B_{bk}/B %
Lc1	90.16%	10.33%
Lc2	77.97%	7.51%
Lc3	71.15%	6.10%
Lc4	64.53%	5.16%
Lc5	*58.97%*	*4.23%*
Lc6	*52.14%*	*3.29%*
Lc7	*47.71%*	*2.82%*
Lc8	***40.67%***	***1.88%***
Lc9	***35.22%***	***1.41%***
Lc10	***31.75%***	***1.41%***
Lc11	***19.33%***	***0.94%***
Lc12	***12.59%***	***0.47%***

extreme case on bilge keel design for a boat, which extended the bilge keel significantly forward towards the bow to reduce heavy rolling. The roll motion of that boat was reduced as expected, but the pitch motion increased dramatically. After an investigation, they found the large pitch motion was caused by the longitudinal position of the bilge keel being installed one-quarter of the boat's length from the bow. The large pitch motion fell back to the original value when they removed the bilge keels from the front one-quarter region. Thus, the position of one-quarter of the boat length from the bow of the EJFB is the front limit of bilge keel design of the present study. According to the recommendations above, the longitudinal locations of each length option are determined and shown in Fig. 12.

4.1.3. Width of bilge keel

The width (or span) of bilge keels is normally between 3% and 5% of the boat's breadth (Sabuncu, 1983). Avalos et al. (2014) used 4% of the boat's breadth for their roll damping decay experiment and simulations. Thiagarajan and Braddock (2010) tested the width effect of bilge keels on the roll damping from 1.2% to 10% of the boat's breadth. When the widths of the bilge keels were too small (i.e. within 2% of the boat's breadth), they may fully immerse into the boundary layer of the boat hull and significantly affect its performance with regards to roll stabilization (Sabuncu, 1983). In the present study, the suggestion from Sabuncu (1983) is considered to select four bilge keel widths (B_{bk}) for further study, which are 2%B, 3%B, 4%B and 5%B in this paper.

4.1.4. Candidate bilge keel design cases

With the parameters discussed above, twelve transverse locations have been selected, five lengths and four widths, which results in 240 candidate bilge keel design cases for further investigation. The parameters of these 240 cases are summarised in Table 5.

Table 5
Parameter range for 240 bilge keel candidate design cases.

12 transverse locations Lc_{bk}/T	5 lengths Lt_{bk}/L	4 width B_{bk}/B
90.2%–12.6%	25.0%; 37.5%; 50.0%; 62.5%; 75.0%	2.0%; 3.0%; 4.0%; 5.0%

4.2. Further criteria for bilge keel design

In this section, further design criteria are applied to the 240 bilge keel candidate design cases, so as to screen out unsuitable designs.

4.2.1. Width criteria for bilge keel design

As a rule of thumb, the width of the bilge keel should not be so large that it exceeds the boat's envelope (Cox and Lloyd, 1977; Sabuncu, 1983). The risk of grounding will be increased if the bilge keel exceeds the baseline of the boat. Rubbing accidents may occur during a boat's encounters if the bilge keel exceeds the extreme breadth of the boat. With this criterion in mind, the maximum bilge keel width allowed within the boat envelope was calculated for each transverse location as shown in Table 4. The maximum bilge keel width allowed within the boat envelope for LC8 to LC12 is smaller than 2%*B* - too small to have a remarkable roll stabilization performance. Thus, these five transverse locations and corresponding 100 design cases were removed from the candidate list. The maximum bilge keel width allowed within the boat envelope for LC5 to LC7 is between 2%*B* and 5%*B*, thus screening out some of the cases with larger B_{bk}/B values.

4.2.2. Resistance estimation and bilge keel design criteria for resistance

It is widely accepted that the major drawback of bilge keels is the increase in resistance during their operation at sea. However, the additional resistance from a bilge keel could be well controlled through precise and rigorous design. Due to that fact that bilge keels are designed to align with the flow streamlines, the resistance of bilge keels can be considered to consist solely of the frictional resistance due to the added wetted surface area of bilge keels, as reported by Taylor (1910); Bhattacharyya (1978) and Lloyd (1989). The alignment of bilge keels was achieved for all bilge keel candidate design cases in the present study through CFD simulations and corresponding post-process visualization technique as shown in Section 4.1.1.

Following the ITTC recommendation, the resistance increment due to bilge keels (δR_{bk}) is estimated by the following conceptual equation in the design stage of the present study (Molland et al., 2017):

$$\delta R_{bk} = \frac{S + S_{bk}}{S} \tag{21}$$

where S and S_{bk} are the wetted surface area of the bare EJFB and bilge keels, respectively.

Taylor (1910) mentioned that the total appendages resistance (including bilge keels, struts and dockings) for a twin screw vessel should around 20% of the resistance of bare hull. Molland et al. (2017) suggest that the resistance increased by bilge keels should be around 2%–3% of the total resistance of the bare hull. In the present study, the resistance increases by bilge keels are maintained below 3% of the bare hull's resistance. With estimations from the conceptual equation above, 20 bilge keel design cases were identified with a 2% resistance increase and 29 bilge keel design cases were identified with a resistance increase between 2% and 3%. Thus, these 49 cases were selected for the roll motion calculation to estimate the roll stabilization performance.

4.3. Roll stabilization of bilge keel design cases in regular waves

The equations presented in Section 2.1 were used to evaluate the boat roll responses in regular waves in the frequency domain for the 49 candidate bilge keel designs as selected in Section 4.2.1. The results of roll responses in regular waves for each case will serve as the primary basis for selecting the final bilge keel design. It is worth reiterating that ShipX was used as a numerical tool to calculate the seakeeping performance of the boat with and without bilge keel.

Fig. 13 (a) shows typical calculation results of the roll responses in regular waves of the roll-stabilized-EJFB with bilge keel Case #1 ($Lt_{bk}/L = 25\%$, $B_{bk}/B = 2\%$ and $Lc_{bk}/T = 90.2\%$) at service speed and compared with that of the bare EJFB. It can be seen that the peak roll response at 45° wave heading has a 29.2% reduction. A 23.8% reduction in the peak roll response is also reached at 90° wave heading. A little reduction in the roll response was achieved at 135° wave heading. The roll responses for the EJFB were not affected by bilge keels at long waves for all wave headings. The roll motion reduction in the peak roll response at 45° wave heading was chosen to be the most significant since it is the most dangerous condition for EJFB during its operation. The effectiveness of peak roll reduction at 45° wave heading (η_{r_45}) is defined to quantify the performance of bilge keels (Cox and Lloyd, 1977):

$$\eta_{r\_45} = 1 - \frac{\eta_{4\_s}}{\eta_{4\_u}} \tag{22}$$

where both η_{4_s} and η_{4_u} represent the peak roll response at 45° wave heading. Subscripts *s* and *u* indicate stabilized and unstabilized results, respectively, by the bilge keels.

Fig. 13 (b) shows the effectiveness of peak roll reduction at 45° wave heading against the width and transverse location at $Lt_{bk}/L = 25\%$. Fig. 13 (c) shows the effectiveness of peak roll reduction at a 45° wave heading against the length and transverse location at $B_{bk}/B = 2\%$. The results indicate that the effectiveness of peak roll reduction increases with increasing bilge keel width and length, which is in agreement with the findings of Thiagarajan and Braddock (2010). Based on the obtained results, it can be said that the effectiveness of peak roll reduction increases with increased averaged transverse distance from baseline. Referring to the hull shape of the EJFB in Fig. 8, the anti-roll moment arm of the bilge keel increases when moving it from the boat baseline towards the free surface along the girth line, which could be the reason for the increase of η_{r_45} for a larger Lc_{bk}/T.

Fig. 13 (d) illustrates the results of the effectiveness of peak roll reduction at a 45° wave heading against the increase of the resistance. The ideal design should have a large η_{r_45} value, but small δR_{bk}, which should be located at the left-top corner (Case #1). On the other hand, the worst case has a completely opposite performance (Case #133) ($Lt_{bk}/L = 62.5\%$, $B_{bk}/B = 2\%$ and $Lc_{bk}/T = 47.7\%$), with a relatively small η_{r_45} value but large δR_{bk}. Since the bilge keel cases are designed based on the flow streamline of the EJFB during the cruising stage at service speed, some of the bilge keel design cases will cross the free surface and be out of the water during accelerating, decelerating and standby stages when the boat has a small or even zero forward speed. In Fig. 13 (d), the result is marked as a green circle if that bilge keel will fully immerse in the water at any speed. Otherwise, the result is marked as a red triangle. As mentioned in Section 4.1.1, it is necessary to keep the bilge keel fully immersed in the water at all times to avoid any additional wave-making resistance. Thus, Case #41 ($Lt_{bk}/L = 25\%$, $B_{bk}/B = 2\%$ and $Lc_{bk}/T = 71.2\%$) with a 26.4% roll motion reduction and a 1.17% resistance increase, was selected for the final design instead of Case #1.

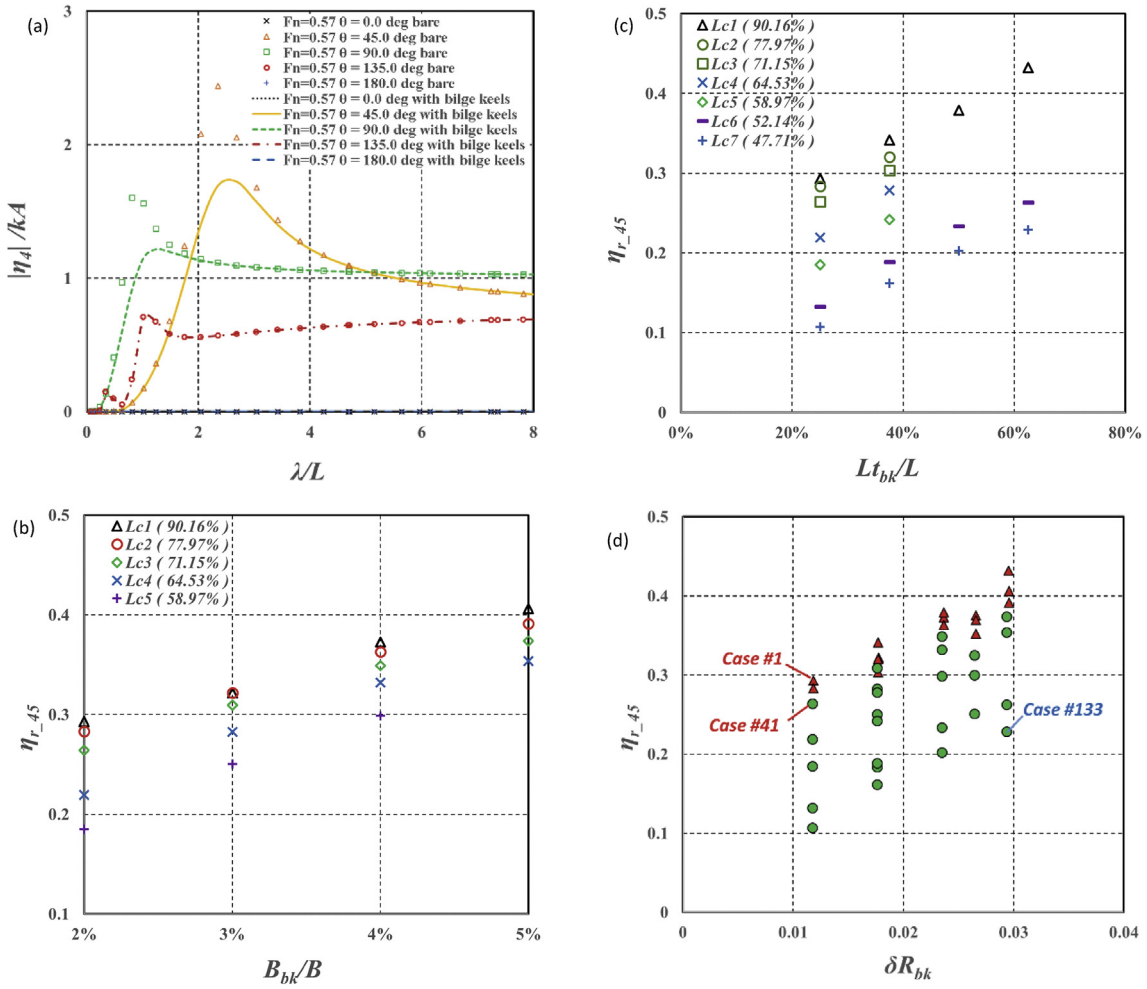

Fig. 13. Results of the roll motion calculation in regular waves for the candidate bilge keel cases.

4.4. Final design of bilge keels for the EJFB

As discussed in Section 4.3, Case #41 was selected as the final bilge keel design of EJFB. The starboard half of the section data of the final bilge keel design for the EJFB is listed in Table 6. The sections of the bilge keel are numbered from the boat stern towards the boat bow. The coordinate of each bilge keel section is defined relative to the local reference frame, where the origin is located at the intersection of the aft-perpendicular, the centerline and the baseline of the boat, with the x-axis pointing forwards from the stern to the bow, the y-axis pointing from port to starboard and the z-axis pointing upwards.

The 3D model of the port side half of the final designed bilge keel and the roll-stabilized-EJFB with the final designed bilge keel are presented in Fig. 14.

Table 6
Section data (starboard half) of the final bilge keel design (Case#41) for the EJFB.

Section No. -	X (m)	Y (m)	Z (m)	Width (m)
1	1.94	0.75	0.16	0.04
2	2.04	0.75	0.17	0.04
3	2.15	0.76	0.18	0.04
4	2.26	0.77	0.2	0.04
5	2.37	0.77	0.21	0.04
6	2.48	0.78	0.22	0.04
7	2.59	0.78	0.24	0.04
8	2.69	0.78	0.26	0.04
9	2.8	0.78	0.27	0.04
10	2.91	0.78	0.29	0.04
11	3.02	0.78	0.31	0.04

5. Analysis of the roll-stabilized-EJFB with the final designed bilge keel

In this section, the roll-stabilized-EJFB with the designed bilge keel is analysed on the roll stability of the real sea state with irregular waves in East Java. The resistance difference due to the installation of bilge keels is also calculated precisely using CFD simulations.

5.1. Performance of the roll-stabilized-EJFB in irregular waves

As mentioned in Section 2.2, the sea state in East Java was modelled by the JONSWAP spectrum with a γ value of 2; the wave height varies from 0.3 m to 1.88 m and the corresponding wave period varies from 7 s to 9 s (Djatmiko, 2015). The standard deviation of roll response to the roll-stabilized-EJFB with the final designed bilge keel (Case #41) in aforementioned sea states at the 45° wave heading condition was calculated and are presented against different significant wave heights with a comparison to a bare EJFB in Fig. 15. The performance of the bilge keel in reducing RMS roll motions was calculated using ShipX for varying sea states,

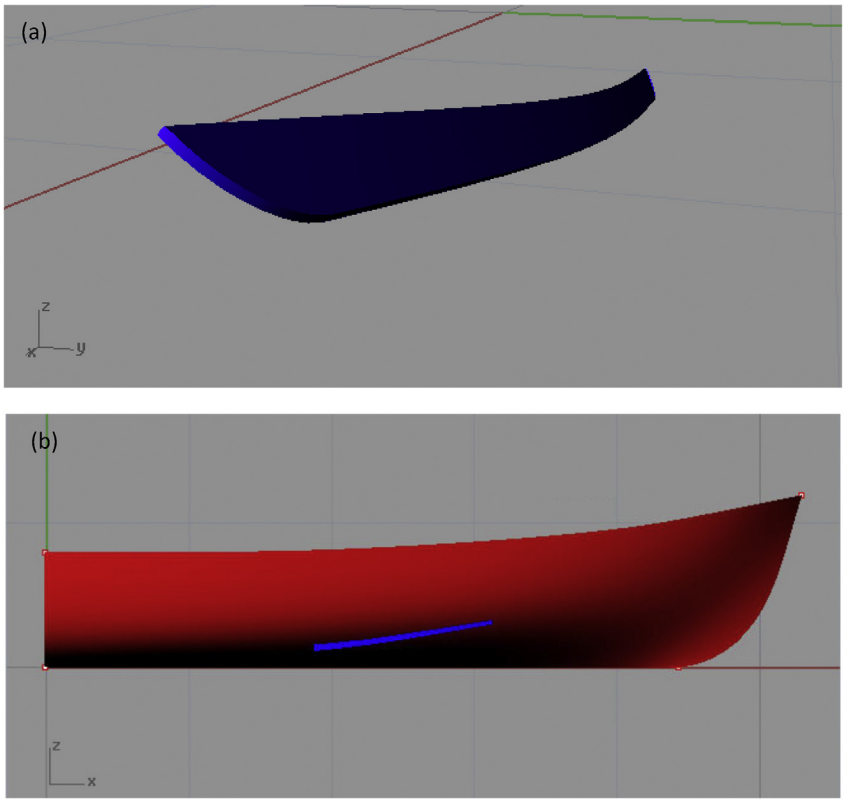

Fig. 14. The final design of (a) bilge keel model (port half) and (b) side view of the roll-stabilized-EJFB with the final design of bilge keel (Case #41).

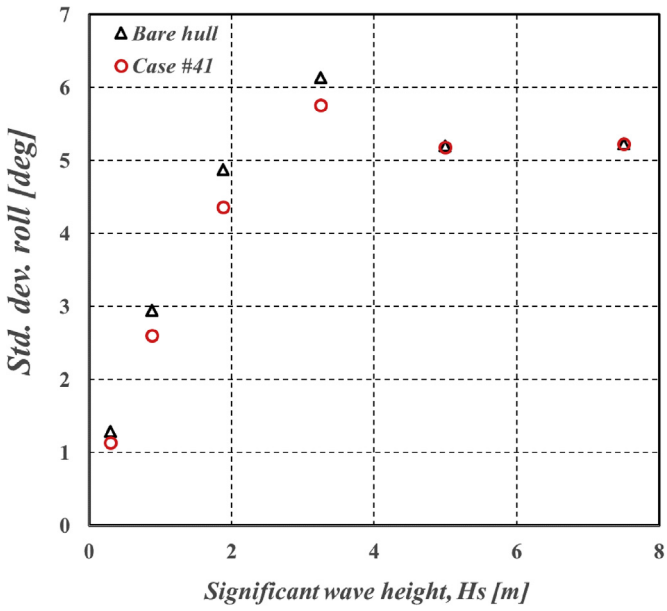

Fig. 15. Results of the roll motion calculation in irregular waves at 45° wave heading for the roll-stabilized-EJFB with the final designed bilge keel.

as shown in Table 7. Table 7 gives the percentage reduction in the roll displacement of the boat, compared to the ship performance without a bilge keel.

As can be seen in Table 7, a remarkable decrease in the standard deviation of roll response was achieved for the roll-stabilized-EJFB with the designed bilge keel at small significant wave heights ($Hs < 4$ m) in the East Java sea. Up to 11.78% reduction could be achieved in the standard deviation of roll response in sea state 2. The results also revealed that the effect of the bilge keel on the roll motion lessens as the number of sea states increases.

Table 7
Standard deviation decrease in the roll response at each significant wave height for the roll-stabilized-EJFB with the final designed bilge keel (Case#41).

Sea State No [−]	Significant wave height, Hs [m]	Std. dev. roll decrease [%]
2	0.3	11.78%
3	0.88	11.41%
4	1.88	10.60%
5	3.25	6.15%
6	5	0.30%
7	7.5	0.04%

The results displayed in Table 7 have proved the effectiveness of the designed bilge keel on the roll stability enhancement. The results also indicate that the designed bilge keel fully meets the objectives and expectations of the present study.

5.2. CFD simulations on the resistance of roll-stabilized-EJFB

During the design stage, an ITTC recommended empirical equation was used to estimate the resistance increase of the roll-stabilized-EJFB compared with the bare EJFB. Since the estimation equation does not take into account any complex interactions between fluid flow and the boat hull, there is a need to accurately calculate/simulate the resistance increase of the roll-stabilized-EJFB. In this section, CFD simulations are used to precisely calculate the influence of bilge keels in terms of the resistance increase at the service speed in calm water.

Fig. 16 (a) shows the simulated total resistance coefficient results for five different cases. Apart from the bare EJFB and the roll-

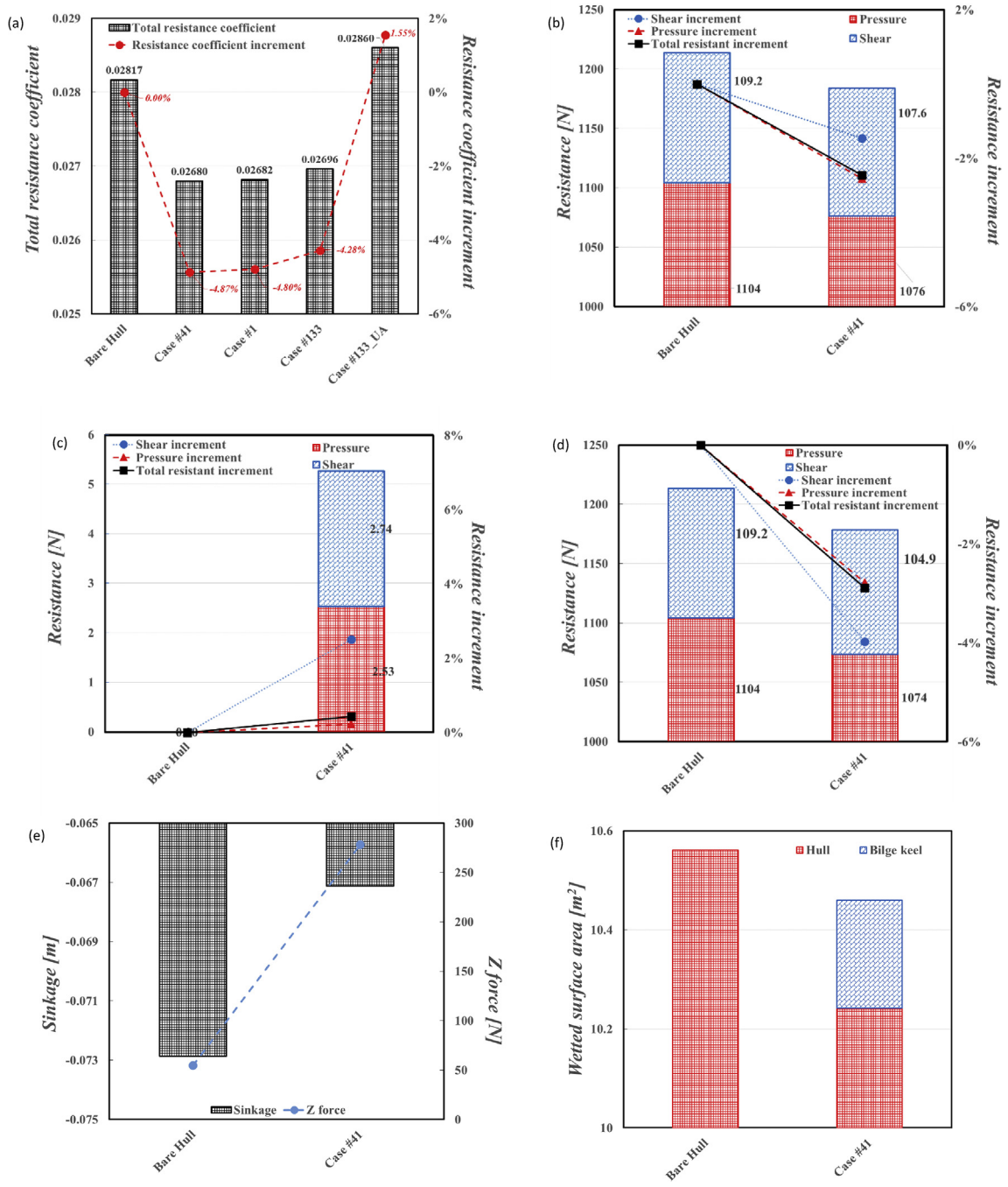

Fig. 16. CFD simulation results on the resistance of bilge keel cases.

stabilized-EJFB with the final design (Case #41), three other bilge keel designs (Case #1, Case #133 and Case #133_UA) were also calculated for comparison purposes, where Case #133_UA represents the modified design of Case #133 with the shape of the bilge keel unaligned with the flow streamlines. The total resistance coefficient of the boat is defined as

$$C_T = \frac{R_T}{\frac{1}{2}\rho U^2 S} \tag{23}$$

where R_T is the total resistance of the boat, including the resistance from bilge keels if installed, ρ is the density of the water; U is the service speed of the boat and S is the wetted surface of the boat.

As can be seen from Fig. 16 (a), the total resistance coefficient of EJFB shows a 4.87% reduction after being roll stabilized by bilge keel Case #41. Fig. 16 (b) – (d) illustrates the breakdown of the resistance components for the entire roll-stabilized-EJFB boat with the bilge keel of Case #41, bilge keel of Case #41 only and the EJFB hull form only, respectively. Both shear and pressure components of the total boat resistance decreased with the installation of bilge keel Case #41. The pressure component plays a dominant role in the total resistance of the entire boat and has a larger resistance decrease than that of the shear component. The shear component accounted for 52% of the resistance from the bilge keels only and

showed positive contributions to the resistance increase of the entire boat. The pressure component accounted for 91% (i.e. the major part) of the total resistance of the hull form only. It has a 1.19% smaller on the resistance decrease than that of the shear component. Since the resistance increased by the bilge keels is smaller than the resistance decrease from the hull form, the total resistance of the entire boat decreases as shown in Fig. 16 (b) and (a).

Fig. 16 (e) shows the sinkage and hydrodynamic forces in the z-axis direction of the roll-stabilized-EJFB with the bilge keel of Case #41 and compared with the bare EJFB. It can be seen that by installing the bilge keel, an extra hydrodynamic force in the z-axis direction is provided, which is about 4.5 times the z-axis hydrodynamic forces for the bare EJFB. As a result, the sinkage of the roll-stabilized-EJFB with the Case #41 bilge keel reduces by 8.2%. Fig. 16 (f) shows the wetted surface area of the roll-stabilized-EJFB with the bilge keel of Case #41 and compared with the bare EJFB. Despite the wetted surface area increasing due to the installation of bilge keels, the overall wetted surface area of the roll-stabilized-EJFB is reduced compared with the bare hull with the extra hydrodynamic force in the z-axis direction. This reveals the reason for the total resistance decreasing for the roll-stabilized-EJFB as in Fig. 16 (a).

It can be seen from Fig. 16 (a) that by installing the bilge keels of Case #1 and Case #133, the total resistance coefficient of the EJFB has decreased as well, because of the same wetted surface reduction effect as that of the bilge keel Case #41. The bilge keel Case #41 has the lowest the total resistance coefficient among these three bilge keel design cases, which is consistent with the recommendations made by the ITTC suggested formula for the bilge keel added resistance.

Compared with bilge keel Case #133, the total resistance coefficient of the roll-stabilized-EJFB with bilge keel Case #133_UA has a value of 0.02860, which is 1.55% larger than the bare EJFB. The extra resistance generated by bilge keel Case #133_UA comes from the pressure forces acting on the unaligned bilge keel due to the angle between the bilge keel and the fluid flow. This proves the importance of the alignment of the bilge keel to the flow streamlines.

6. Concluding remarks

In this paper, a state-of-the-art bilge keel design method was applied using numerical and semi-empirical formulae to design bilge keels for EJFB. 240 different design cases for bilge keels were assessed and shortlisted for the EJFB based on parameter selection. By applying the formulae, roll amplitudes of the EJFB with these candidate bilge keel cases in the frequency domain were calculated. The added resistance of the EJFB with these candidate bilge keel cases was also estimated by applying the semi-empirical formula, as recommended by ITTC, during the design stage. With the conceptual calculations above, the present study identified the final design of the bilge keel, which can contribute to significant roll damping but provide only a small added resistance to the boat hull. After installing the bilge keels, up to 26.4% reduction could be achieved for the roll motion for the roll-stabilized-EJFB in regular waves and up to 11.78% reduction in the standard deviation of roll response could be reached in irregular seas. The total resistance has a 1.17% increase following installation of the bilge keel, which was estimated by the semi-empirical formula.

The present study also employed a state-of-the-art CFD method, which involves numerical simulations offering higher accuracy than semi-empirical formulae, to accurately simulate the total resistance increment of the fishing boat with the designed bilge keel. The results show that the bilge keel could provide extra forces to reduce the sinkage of the boat, so as to reduce its wet surface and the total resistance coefficient. Thus, the installation of bilge keels results in a 4.87% reduction of the total resistance coefficient. The results also demonstrated the necessity of aligning the bilge keel with the flow streamline, so as to reduce the resistance of the bilge keel.

This study established the best practices for a seakeeping analysis on the EJFB and designed bilge keels for this fishing boat to enhance its safety level in terms of roll stability, especially in some extreme weather conditions. Moreover, reduced roll-motion can lead to a decrease in the number of capsize accidents observed yearly. The bilge keel, which was designed in the present study, not only increased the safety of the fishing boat by reducing the roll motion but also reduced the total resistance of the EJFB, leading to reduced fuel consumption for local stakeholders in Indonesia.

By using the new EJFB with bilge keels that designed in the present paper not only enhanced the boats' safety but also reduced the total resistance of the boats, resulting in increased operational efficiency and reduced fuel costs as well as emissions for local stakeholders.

The present study employed the state-of-the-art bilge keel design method with numerical simulations and semi-empirical formulae for EJFB. Due to the limited budget and resources of this present project, future studies will investigate bilge keel design and analysis using model tests, and large-scale and full scale tests will also be carried out.

Acknowledgments

This research project is funded by the Institutional Links Grants (Grant ID: 217539254) of the British Council.

The authors would like to thank the valuable discussions and suggestions provided by Prof Mehmet Atlar and valuable help from Mr Anthony Romanowski. The authors would like to thank Dr Holly Yu for her help with the final proofreading.

CFD results were obtained using the EPSRC funded ARCHIE-WeSt High-Performance Computer (www.archie-west.ac.uk). EPSRC grant no. EP/K000586/1.

References

Arslan, Volkan, Kurt, Rafet Emek, Turan, Osman, Wolff, Louis De, 2016. Safety culture assessment and implementation framework to enhance maritime safety. Trans.Res.Procedia 14, 3895–3904.

Avalos, Gustavo OG., Wanderley, Juan BV., Fernandes, Antonio C., Oliveira, Allan C., 2014. Roll damping decay of a FPSO with bilge keel. Ocean. Eng. 87, 111–120.

Bassler, Christopher C., Reed, Arthur M., 2009. An analysis of the bilge keel roll damping component model. In: Proc. 10th Intl. Conf. Stability of Ships and Ocean Vehicles.

Bhattacharyya, Rameswar, 1978. Dynamics of marine vehicles. Ocean. Eng.Awiley 278–307.

CD-Adapco, 2014. In: User Guide STAR-CCM+ Version 9.0.2. CD-adapco, Melville, NY.

Celik, I.B., Ghia, U., Roache, P.J., Freitas, C.J., 2008. Procedure for estimation and reporting of uncertainty due to discretization in CFD applications. J. Fluid Eng.-Trans. ASME 130, 078001.

Chakrabarti, Subrata, 2001. Empirical calculation of roll damping for ships and barges. Ocean. Eng. 28, 915–932.

Cox, Geoffrey G., Lloyd, Adrian R., 1977. In: Hydrodynamic Design Basis for Navy Ship Roll Motion Stabilization. Published Report.

Demirel, Yigit Kemal, Turan, Osman, Incecik, Atilla, 2017. Predicting the effect of biofouling on ship resistance using CFD. Appl. Ocean Res. 62, 100–118.

Djatmiko, Eko Budi, 2015. In: Perilaku dan Operabilitas Bangunan Laut di Atas Gelombang Acak. Published Book.

Dove, 1958. In: Effect of Bilge Keel Position on Roll Damping in Frigates. Unpublished MOD (PE) Report.

Enger, S., Peric, M., Peric, R., 2010. Simulation of flow around KCS-hull. In: Gothenburg 2010-A Workshop on Numerical Ship Hydrodynamics. Gothenburg.

Fathi, Dariusz, Hoff, Jan Roger, 2004. Shipx Vessel Responses (Veres)', Theory Manual, Marintek AS, Feb, 13.

Ferziger, J.H., Peric, M., 2002. Computational Methods for Fluid Dynamics. Springer, Berlin, Germany.

Himeno, Yoji, 1981. Prediction of Ship Roll Damping-a State of the Art. Thesis of

University of Michigan).
Ikeda, Yoshiho, Himeno, Yoji, Tanaka, Norio, 1977. On eddy making component of roll damping force on naked hull. J. Soc. Nav. Archit. Jpn. 1977, 54–64.
Journée, J.M.J., 1992. Experiments and calculations on 4 Wigley hull forms in head waves. In: Delft University of Technology. Report, 909.
Kim, S.P., Lee, H.H., 2011. Fully nonlinear seakeeping analysis based on CFD simulations. In: 21st International Offshore and Polar Engineering Conference, 970–74. Hawaii, USA.
Liu, Wendi, Baihaqi, Imam, Tezdogan, Tahsin, Emek Kurt, Rafet, Nugroho, Setyo, Yuan, Zhiming, Supomo, Heri, Kemal Demirel, Yigit, Budi Djatmiko, Eko, Incecik, Atilla, 2016. Designing safe, green and sustainable vessels for Indonesian coastal transport and fishing operations. In: The 1st International Conference on Marine Technology (SENTA).
Lloyd, A.R.J.M., 1989. Seakeeping: Ship Behaviour in Rough Weather. Published Report.
Lofft, 1973. RFA Engadine: Effect of Bilge Keels on Rolling and Motion in Head Seas, 16/73. Admiralty Experiment Works Report.
Molland, Anthony F., Turnock, Stephen R., Hudson, Dominic A., 2017. Ship Resistance and Propulsion. Cambridge university press.
OGP, 2010. Water transport accident statistics. Int. Assoc. Oil & Gas Prod., 434-10
Perez, Tristan, Blanke, Mogens, 2010. Ship roll motion control. In: IFAC Conference on Control Applications in Marine Systems.
Richardson, L.F., 1911. The approximate arithmetical solution by finite differences of physical problems involving differential equations, with an application to the stresses in a Masonry dam. Philos. Trans. R. Soc. Lond. - Ser. A Contain. Pap. a Math. or Phys. Character 210, 307–357.
Richardson, Lewis F., Gaunt, J Arthur, 1927. The deferred approach to the limit. Part I. Single lattice. Part II. Interpenetrating lattices. Philos. Trans. R. Soc. Lond. - Ser. A Contain. Pap. a Math. or Phys. Character 226, 299–361.
Sabuncu, Tarık, 1983. Gemi Hareketleri (İTÜ). Published Book.
St Dinis, M., Pierson Jr., W.J., 1953. On the motions of ships in confused seas. Trans. Soc. Nav. Archit. Marine Eng. 61, 280–357.
Taylor, David Watson, 1910. The Speed and Power of Ships: a Manual of marine Propulsion. Published Book.
Tezdogan, Tahsin, Kemal Demirel, Yigit, Kellett, Paula, Khorasanchi, Mahdi, Incecik, Atilla, Turan, Osman, 2015. Full-scale unsteady RANS CFD simulations of ship behaviour and performance in head seas due to slow steaming. Ocean. Eng. 97, 186–206.
Tezdogan, Tahsin, Incecik, Atilla, Turan, Osman, 2014. Operability assessment of high speed passenger ships based on human comfort criteria. Ocean. Eng. 89, 32–52.
Thiagarajan, Krish P., Braddock, Ellen C., 2010. Influence of bilge keel width on the roll damping of FPSO. J. Offshore Mech. Arctic Eng. 132, 011303.
Turan, Osman, Emek Kurt, Rafet, Arslan, Volkan, Silvagni, Sara, Ducci, Marco, Liston, Paul, Maarten Schraagen, Jan, Fang, Ivy, Papadakis, George, 2016. Can we learn from aviation: safety enhancements in transport by achieving human orientated resilient shipping environment. Trans.Res.Procedia 14, 1669–1678.
Yuan, Zhi-Ming, Incecik, Atilla, Jia, Laibing, 2014. A new radiation condition for ships travelling with very low forward speed. Ocean. Eng. 88, 298–309.